Journal of Solid State Chemistry **144,** 62–67 (1999)
Article ID jssc.1998.8118, available online at http://www.idealibrary.com on IDEAL®

Structure of $TlSr_2NiO_{4+\delta}$ by High-Resolution Neutron Powder Diffraction

C. S. Knee and M. T. Weller[1]

Department of Chemistry, University of Southampton, Southampton SO17 1BJ, United Kingdom

Received June 24, 1998; in revised form October 27, 1998; accepted December 7, 1998

$TlSr_2NiO_{4+\delta}$ has been synthesized and its structure determined using high-resolution neutron powder diffraction data collected at 5 K, 90 K, and room temperature. It crystallizes in an orthorhombic cell, space group *Pmmm*, lattice parameters $a = 3.7217(1)$, $b = 7.5158(2)$, and $c = 8.8321(3)$ Å. The compound is isostructural with the orthorhombic form of $TlSr_2CuO_y$, with alternating TlO and oxygen-deficient NiO_{2-x} layers connected through oxygen. Ordering of the oxygen vacancies in the NiO_{2-x} layer occurs, producing a superstructure with alternating NiO_6 octahedra and NiO_4 square planes along the *b*-direction. A comparison between the nickel and copper environments in the two materials is performed. Magnetic susceptibility data reveal that $TlSr_2NiO_{4+\delta}$ displays Curie–Weiss behavior in the range 80–300 K with a weak antiferromagnetic ordering at 15 K.

Key Words: **neutron diffraction; $TlSr_2NiO_{4+\delta}$; orthorhombic $TlSr_2CuO_y$; oxygen vacancies; superstructure.**

INTRODUCTION

The structural chemistry of complex nickelates has recently regained impetus from its relationship with that of cuprates exhibiting high-temperature superconductivity. Of particular interest have been complex nickel oxides adopting the perovskite and K_2NiF_4 structures which show magnetic and electrical similarities to the corresponding cuprates, e.g., $La_{2-x}Sr_xMO_{4\pm\delta}$ (M = Ni, Cu) (1, 2). A few other phases exist with structural analogies in copper and nickel chemistry, for example, Li_2MO_2 (3, 4) and "$BaMO_2$" (5, 6). These structural analogues derive from the ability of both copper(II) and nickel(II) to adopt four-fold (square planar), fivefold (square pyramidal), and sixfold (octahedron based) coordinations to oxygen though the five- and sixfold geometries are normally more distorted for copper due to the Jahn–Teller effect. More recently the synthesis of a series of structurally related compounds (7) with nickel present in the higher oxidation state of 3+ have been reported.

[1]To whom correspondence should be addressed. Fax: 00 44 1703 593592. E-mail: mtw@soton.ac.uk.

In addition to the formation of pure nickel analogues of copper materials, there have been numerous doping studies performed on high-T_c cuprate phases that involved the substitution of nickel for copper (8–10). These studies generally indicate a solubility of nickel between 0 and 10%, and invariably the doping has a deleterious effect on the superconducting transition temperature T_c. One of the most important high-T_c series of materials is the thallium-stronium calcium copper oxides $TlSr_2Ca_{n-1}Cu_nO_{3.5+2n}$ with $n = 1, 2, 3, 4$ (11, 12). The $n = 1$ member $TlSr_2CuO_y$ occurs in tetragonal and orthorhombic forms depending on the synthesis conditions. The tetragonal phase was reported in a single-crystal study (13) and becomes superconducting when suitable doping of the phase is performed, e.g., $TlSr_{2-x}La_xCuO_y$ (14). The polycrystalline orthorhombic form has been reported by Ganguli and Subramanian (15), but no superconducting transition is observed in this form of the material. Further structural analysis of this phase revealed the presence of partially ordered oxygen vacancies in the CuO_{2-x} layer (16). The ordering of the vacancies were found to be consistent with a $2b$ superstructure, resulting in alternating CuO_6 octahedra and CuO_4 square planes along the b direction. A tetragonal cobalt analogue $TlSr_2CoO_5$ has been reported though the material as prepared seems always to exist as a mixture of two structurally similar phases (17), making full structural characterization difficult.

In this paper we report the detailed structure determination, by high-resolution neutron diffraction, of $TlSr_2NiO_{4+\delta}$, a nickel analogue of orthorhombic $TlSr_2CuO_y$. Details of the synthesis of the material and a preliminary structure determination, using powder X-ray diffraction, have been communicated previously (18). The magnetic properties of the material are also discussed in relation to its crystal structure and a structural comparison with $TlSr_2CuO_y$ is made.

STRUCTURE REFINEMENT

Powder X-ray Diffraction Data

The structure of $TlSr_2NiO_{4+\delta}$, as refined from powder X-ray diffraction data using the GSAS package (19), has

0022-4596/99 $30.00

been communicated previously. The starting structural model for that refinement was proposed by Ganguli and Subramanian (15) for orthorhombic $TlSr_2CuO_5$, space group *Pmmm*, cell parameters $a = 3.700$, $b = 3.770$, $c = 8.850$ Å, all atoms at full occupancy. Thallium is situated on (0, 0, 0), nickel on (0, 0, 0.5), strontium on (0.5, 0.5, z), $z = 0.295$, and oxygen atoms on (0, 0, z), $z \approx 0.25$, O(1); 0, 0.5, 0.5), O(2); (0.5, 0.5, 0), O(3); and (0.5, 0, 0.5), O(4). O(2) and O(4) lie in the same plane as nickel, producing for full occupancy layers of the stoichiometry NiO_2; O(3) coordinates four-fold to the thallium atom, producing TlO_2 layers; and O(1) formally connects the nickel and thallium levels.

Refinement of the model resulted in the displacement of the thallium from the origin onto a partially occupied (x, y, 0) site with $x \approx y \approx 0.05$ and a decrease in the total unit cell occupancy to approximately 0.75. Attempts to disorder or partially occupy the neighboring O(3) atom were unsuccessful. The fractional occupancy of the O(2) and O(4) oxygen atoms was allowed to vary and refined stably to 0.8 and 0.5, respectively, representing oxygen-deficient NiO_{2-x} planes. A small level of nickel oxide impurity ($I/I_0 < 5\%$) was included in the profile refinement using literature data. The final refined temperature factor associated with the O(1) oxygen was large but attempts to disorder/partially occupy the site produced unstable refinements due to the insensitivity of X-ray diffraction data to the light oxygen atoms. The overall goodness-of-fit parameters obtained were only reasonable, i.e., $R_p = 10.8\%$, $R_{wp} = 14.2\%$, and $\chi^2 = 17.2$, indicating some deficiencies in the structural model.

Neutron Powder Diffraction Data

Data collection. Approximately 2 g of sample was placed in a 6-mm-diameter vanadium can and cooled to 5 K in a standard ILL cryostat. The powder pattern was collected at steps of $2\theta = 0.05^\circ$ over the range 0°–160° on the high-resolution, constant-wavelength ($\lambda = 1.911$ Å) neutron powder diffractometer D1A over a period of 8 h. Two further patterns were collected at 90 and at 300 K. Temperature control of 1° was achieved for each of the three scans.

Refinement of 5 K data. The neutron powder diffraction pattern was refined, again using the GSAS program, and the same starting structural model as detailed above for the X-ray refinement. The nuclear scattering lengths used were 8.878 fm (Tl), 10.300 fm (Ni), 7.020 fm (Sr), and 5.805 fm (O) (20). Initial stages of the refinement included background parameters, histogram scale factor, peak shape, lattice parameters, and zero point displacement. The small level of NiO impurity present in the sample was fitted using literature data and refinement of lattice constants and the phase fraction only.

Introduction of atomic and thermal parameters for all atoms into the refinement produced a relatively poor fit to the data. Temperature factors for the Tl, O(1), O(3), and O(4) atoms refined to unreasonably large values, indicating site disorder and/or partial occupancy. To attempt to improve the profile fit, the refinement proceeded with the displacement of the thallium atom onto a four-fold site (x, y, 0) and a reduction in the site occupancy to 0.85. The neighboring in-plane O(3) atom was found to favor a disordered site at $(0.5 + \delta,\ 0.5 + \delta, 0)$, $\delta \approx 0.055$. Next the occupancy of the O(4) site, which lies in the NiO_2 plane along the a direction, was allowed to vary and refined to 0.65. Finally the O(1) atom which connects the TlO and NiO_2 layers was investigated. The site occupancy was allowed to vary, but this failed to improve the profile fit; therefore an anisotropic temperature factor was introduced. This produced a significant improvement to the profile fit; however, the z component (U_{33}) of the temperature factor refined to an unacceptably large value ~ 10 Å^2, implying vertical disorder of the site. Ohshima *et al.* (16), in their analysis of $TlSr_2CuO_y$, also observed a larger than expected z component (U_{33}) of the equivalent O(1) oxygen's anisotropic thermal parameter. This, combined with HREM evidence, led them to perform a second analysis with a doubled-b superstructure. The possibility of a larger unit cell with a $2b$ lattice for $TlSr_2NiO_{4+\delta}$ was therefore investigated, and close inspection of the diffraction profile revealed two weak reflections consistent with a unit cell $a \times 2b \times c$.

The Superlattice Model

A new structural model was introduced, using the atomic coordinate description proposed by Ohshima *et al.* (16) for $Tl_2Sr_4Cu_2O_y$. The same space group, *Pmmm*, was used with a doubled-b parameter. Eleven atomic sites were contained in the new orthorhombic unit: Tl(1) at (0, 0, 0), Tl(2) at (0, 0.5, 0), Sr at (0.5, y, z), Ni(1) at (0, 0, 0.5), Ni(2) at (0, 0.5, 0.5), O(1) at (0.5, y, 0), O(2) at (0, 0, z), O(3) at (0, 0.5, z), O(4) at (0, y, 0.5), O(5) at (0.5, 0, 0.5), and O(6) at (0.5, 0.5, 0.5). Preliminary stages of the refinement proceeded as before with the inclusion of global parameters such as the zero point displacement. Before further stages of the refinement were undertaken, the temperature factors of both the nickel atoms and, independently, the oxygen's O(5) and O(6) were linked. These atoms lie on similar sites in the structure and these parameters are likely to be similar and strongly correlated. Atomic and thermal parameters for all atoms were introduced and resulted in unexpectedly large temperature factors for the thallium atoms Tl(1) and Tl(2) and the oxygen sites O(1), O(5), and O(6). Displacement of Tl(1) onto a four-fold (x, y, 0) site refined stably but with the y component reverting to near zero (and fixed at this value in later cycles) and $x \approx 0.069$. The fractional occupancy of Tl(2) was allowed to vary and this refined to 0.78

TABLE 1
Refined Atomic Coordinates for $TlSr_2NiO_{4+\delta}$ at 5, 90, and 300 K

	5 K					90 K					300 K				
	x	*y*	*z*	*B*	*g*	*x*	*y*	*z*	*B*	*g*	*x*	*y*	*z*	*B*	*g*
Tl(1)	0.0687(20)	0	0	0.84(15)	0.5	0.0699(22)	0	0	0.83(17)	0.5	0.0687(22)	0	0	1.37(18)	0.5
Tl(2)	0	0.5	0	0.99(20)	0.78(1)	0	0.5	0	1.16(25)	0.77(2)	0	0.5	0	0.93(22)	0.76(2)
Sr	0.5	0.2488(7)	0.2930(2)	0.39(5)	1	0.5	0.2493(2)	0.2933(2)	0.50(5)	1	0.5	0.2471(8)	0.2927(2)	0.62(4)	1
Ni(1)	0	0	0.5	0.54(5)	1	0	0	0.5	0.55(5)	1	0	0	0.5	0.73(5)	1
Ni(2)	0	0.5	0.5	0.54(5)	1	0	0.5	0.5	0.55(5)	1	0	0.5	0.5	0.73(5)	1
O(1)	0.4546(24)	0.2689(10)	0	1.27(14)	0.5	0.4452(21)	0.2704(10)	0	0.68(15)	0.5	0.4476(21)	0.2681(11)	0	1.19(14)	0.5
O(2)	0	0	0.2381(6)	0.54(12)	1	0	0	0.2403(6)	0.75(16)	1	0	0	0.2406(6)	1.07(15)	1
O(3)	0	0.5	0.2815(6)	0.32(11)	1	0	0.5	0.2793(6)	0.49(15)	1	0	0.5	0.2792(6)	0.72(14)	1
O(4)	0	0.2512(14)	0.5	1.07(8)	1	0	0.2504(15)	0.5	1.00(9)	1	0	0.2494(15)	0.5	1.35(8)	1
O(5)	0.5	0	0.5	0.63(17)	1	0.5	0	0.5	0.54(11)	1	0.5	0	0.5	1.00(11)	1
O(6)	0.5	0.5	0.5	0.63(17)	0.35	0.5	0.5	0.5	0.54(11)	0.37	0.5	0.5	0.5	1.00(11)	0.37
a			3.7112(1)					3.7132(2)					3.7217(1)		
b			7.5007(2)					7.5040(2)					7.5158(2)		
c			8.8141(2)					8.8178(2)					8.8321(3)		

Note. Estimated standard deviations are given in parentheses. Temperature factor *B* in Å^2; *g* is the site occupancy factor. Cell parameters in Å; space group *Pmmm.*

occupation, with a simultaneous reduction in the atom's thermal parameter to an acceptable value. The high-temperature factor associated with the O(1) atom, which lies in the TlO layer, was resolved by allowing the atom to move off the (0.5, *y*, 0) site onto the two-fold (*x*, *y*, 0) site $x \approx 0.45$, $y \approx 0.27$. Finally the occupancy of the O(5) and O(6) atoms was allowed to vary. The O(5) atom fractional occupancy refined to unity while O(6) favored a marked decrease to 0.35 occupancy. The thermal parameter associated with the two atoms was allowed to vary independently of the fractional occupancies of the two sites and refined stably to an acceptable value.

The same refinement process was followed for the data collected at 90 and 300 K. The expected trend of increasing temperature factors and lattice parameters with increasing temperature was observed. The final refined atomic coordinates of $TlSr_2NiO_{4+\delta}$, or more accurately $TlSr_4Ni_2O_{9+\delta}$, are summarized in Table 1. Derived bond lengths and final fit parameters are given in Table 2, and the final fit to the 5 K profiles shown in Fig. 1.

DISCUSSION

The detailed structural characterization of $TlSr_2NiO_{4+\delta}$ using neutron difraction has revealed that the initial subcell model, reported in the communication (18), required modification in terms of the oxygen sublattice. Refinement of the neutron diffraction data, in particular, the introduction of an anisotropic thermal parameter for the apical O(1) oxygen, revealed the presence of a superstructure requiring the doubling of the *b* cell parameter. This behavior mirrors that reported for $TlSr_2CuO_y$ by Ohshima *et al.* (16). Adopting the new unit cell for $TlSr_2NiO_{4+\delta}$ produced a markedly better fit to the profile as well as acceptable thermal parameters for all the atoms.

The idealized crystal structure of $TlSr_2NiO_{4+\delta}$ consists of NiO_6 octahedra and vertically aligned NiO_4 square planes and is shown in Fig. 2. The diagram depicts a perfectly alternating array of octahedra and square planes; however, the refined fractional occupancy of the O(6) site, at around

TABLE 2
Interatomic Distances (Å)

Bond	5 K	90 K	300 K
Tl(1)–O(1) × 8	2.466(8)–2.797(10)	2.462(8)–2.789(10)	2.460(8)–2.784(10)
Tl(1)–O(2) × 2	2.122(5)	2.135(6)	2.140(5)
Tl(2)–O(1) × 8	2.430(10)–2.668(8)	2.388(9)–2.686(7)	2.411(9)–2.695(7)
Tl(2)–O(3) × 2	2.474(5)	2.463(6)	2.466(5)
Sr–O(1) × 2	2.5911(19)	2.5992(22)	2.5977(20)
Sr–O(2) × 2	2.669(4)	2.677(4)	2.669(4)
Sr–O(3) × 2	2.652(4)	2.646(4)	2.663(4)
Sr–O(4) × 2	2.6030(11)	2.6017(13)	2.6104(12)
Sr–O(5)	2.605(4)	2.612(4)	2.608(4)
Sr–O(6)	2.629(4)	2.619(5)	2.639(5)
Ni(1)–O(2) × 2	2.301(5)	2.290(6)	2.291(5)
Ni(1)–O(4) × 2	1.880(11)	1.879(12)	1.874(11)
Ni(1)–O(5) × 2	1.85560(5)	1.85662(5)	1.86083(6)
Ni(2)–O(3) × 2	1.933(5)	1.946(6)	1.950(5)
Ni(2)–O(4) × 2	1.870(11)	1.873(12)	1.884(11)
Ni(2)–O(6) × 2	1.85560(5)	1.85662(5)	1.86083(6)
R_p (%)	4.86	4.88	4.51
R_{wp} (%)	6.31	6.32	5.91
χ^2	2.570	2.625	2.20
R_e (%)	3.94	3.90	3.98
R_F (%)	5.12	5.32	5.80

Note. Estimated standard deviations are given in parentheses. Final goodness-of-fit parameters for the various refinements are also shown.

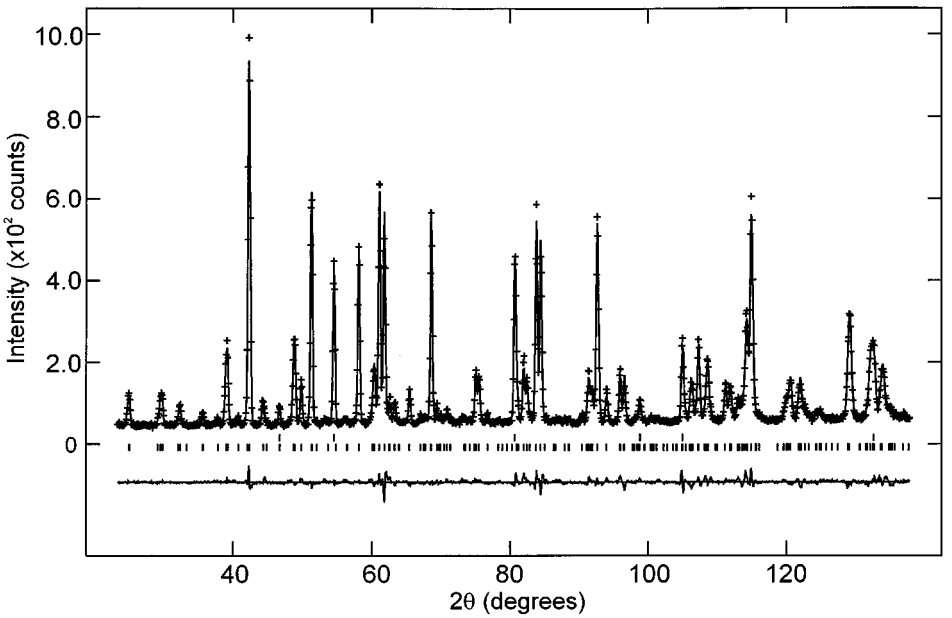

FIG. 1. Final fit achieved to the 5 K powder neutron diffraction data in the 2θ range 22°–145°. Crosses, observed intensities; upper continuous line, calculated profile; lower line, the difference. Upper tick marks show reflections allowed for NiO and lower tick marks show those for $Tl_2Sr_4Ni_2O_{9+\delta}$.

0.35, means that on some occasions the Ni(2) environment will actually be square pyramidal and, very rarely, octahedral. This behavior reflects the structural flexibility of Ni^{2+}/Ni^{3+} which are commonly found in a variety of coordinations due to the low excess octahedral crystal field stabilization energy.

The effects of changing the in-plane nickel coordination number from close to 2 to 4 is reflected in the apical nickel oxygen distance, which changes from 2.291 Å for the Ni(1) atom with the fully occupied basal plane to 1.950 Å for the otherwise weakly, in-plane bonded Ni(2) (see Fig. 3). The $La_{2-x}Sr_xNiO_4$ series ($x \leq 0 \leq 1.6$) (21), in which nickel displays a wide range of oxidation states from +2 to +3.6 and is octahedrally coordinated, provides an interesting comparison. For the $x = 0$ sample, i.e., Ni +2, the apical Ni–O bond length is 1.935 Å; for the $x = 1$, Ni +3, sample, the apical bond contracts to 2.05 Å and the basal bond to 1.913 Å. From Table 3 it is clear that although the apical bonds are reasonably similar given the different

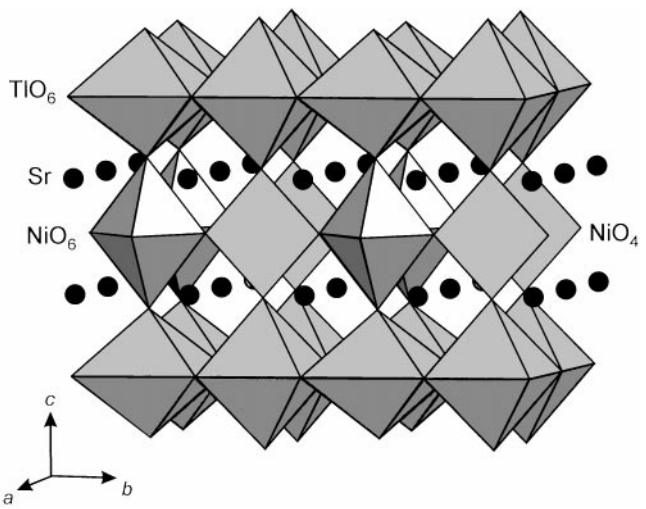

FIG. 2. Idealized structure of $TlSr_2NiO_{4+\delta}$ showing the nickel coordination geometry as an alternating mixture of octahedra and square planes. The thallium coordination is shown as distorted octahedra and the strontium ions are shown as dark spheres.

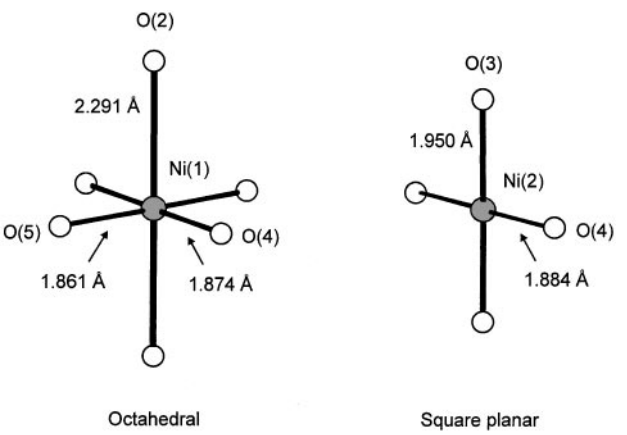

FIG. 3. Illustration of two possible nickel environments—octahedral and square planar—and the effect on the apical Ni–O bond.

TABLE 3
Comparison of the Ni and Cu Environments in the $Tl_2Sr_4M_2O_{9+\delta}$ Materials

Bond (Å)	Ni[a]	Cu[b]
M(1)–O(2)	2.291(5)	2.41(2)
M(1)–O(4)	1.880(11)	1.91(3)
M(1)–O(5)	1.8556(5)	1.8304(3)
M(2)–O(3)	1.950(5)	2.16(4)
M(2)–O(4)	1.870(11)	1.88(3)

Note. Estimated standard deviations are given in parentheses.
[a] 300 K experiment.
[b] Reference (16).

coordination geometries, the Ni–O basal distances $\sim$1.87 Å are substantially shorter in $TlSr_2NiO_{4+\delta}$.

$TlSr_2NiO_{4+\delta}$ exhibits disorder in the TlO layer, with the thallium Tl(1) atom being displaced onto a two-fold site at $(x, 0, 0)$ $x \approx 0.068$, and the neighboring in-plane O(1) favoring a four-fold site at $(x, y, 0)$ $x \approx 0.45$, $y \approx 0.27$. The origin of this disorder is believed to be a result of the need for the rocksalt TlO layer to register with the larger NiO_2 layer. Disorder of this nature is commonly observed in the single-layer thallium copper oxide materials (12, 22). Refinement of the fractional occupancy of Tl(2) revealed an approximate 20% thallium deficiency on this site. The TlO coordination is further complicated by the two apical oxygens' sites O(2) and O(3), and is best described as, on average, distorted octahedral.

The asymmetric distribution of oxygen vacancies in the NiO_{2-x} plane leads to the orthorhombic distortion, i.e., $a = 3.7217(1)$, $b/2 = 3.7579(1)$, $c = 8.8321(3)$ Å (room temperature). Full occupancy of all the oxide sites would require a nickel oxidation state of 3+ and result in infinite NiO_2 layers in the *ab* plane. In fact, assuming all thallium present is 3+, the refined stoichiometry of $Tl_{1.78}Sr_4Ni_2O_{9.36}$ yields a nickel oxidation state of 2.69+; this is fairly typical of a nickel compound synthesized under the conditions described. Attempts to alter the oxygen stoichiometry by annealing samples under various atmospheres, including high-pressure oxygen, have been unsuccessful. The final fit to the observed diffraction pattern (Fig. 1) reveals a less than perfect match and this is reflected in the slightly higher than usual *R* factors obtained in Table 2. The high level of disorder within the structure is believed to be responsible for the discrepancy. Other investigations of 1201 phases have also encountered this problem (14).

Comparison of $TlSr_2NiO_{4+\delta}$ and $TlSr_2CuO_y$

It is interesting to compare the results of the refinements on $TlSr_2NiO_{4+\delta}$ presented herein and the isostructural $TlSr_2CuO_y$ performed by Ohshima *et al.* (16). The nickelate displays a smaller level of disorder in the thallium–oxygen plane with the displacement of Tl(1) onto a two-fold site $(x, 0, 0)$ $x \approx 0.07$, compared with the four-fold site $(x, y, 0)$ $x \approx 0.05$, $y \approx 0.03$, favored by the cuprate. Both materials exhibit a thallium deficiency with a reduction in occupancy of the Tl(2) site. The decrease in thallium is more appreciable for the nickelate, with a thallium occupation of 1.78 compared with 1.95 for the cuprate. $Tl_2Sr_4Cu_2O_y$ also reveals a small level of oxygen deficiency in the Tl–O(1) layer, with the reduction in the oxygen's occupancy to 0.92. A comparison of the local oxygen coordination of the metal ions is shown in Table 3 (also see Fig. 3). These results reveal a greater distortion in the copper environment compared with the nickelate. For example comparing the octahedral apical *M*(1)–O(2) bond length, the Ni–O distance is 2.291(5) and Cu–O distance is 2.41(2) Å. Evaluation of the oxygen occupation yields a copper oxidation state of 2.12+, lower than the 2.69+ value obtained for the nickelate. The larger distortion may therefore be attributed to the propensity of copper(II) to undergo Jahn–Teller effects. Finally, the degree of ordering of the oxygen vacancies is greater for $Tl_2Sr_4Ni_2O_{9+\delta}$, the O(5) site remaining fully occupied and the O(6) falling to 0.37. The occupancy of the O(5) and O(6) oxygens for the cuprate are 0.74 and 0.45, respectively. This may be interpreted as greater segregation of the NiO_6 and NiO_4 structural units throughout the material.

Magnetic Properties

The magnetic susceptibility of $TlSr_2NiO_{4+\delta}$ was measured using a vibrating sample magnetometer over the temperature range 300–4 K and the results are shown in Fig. 4.

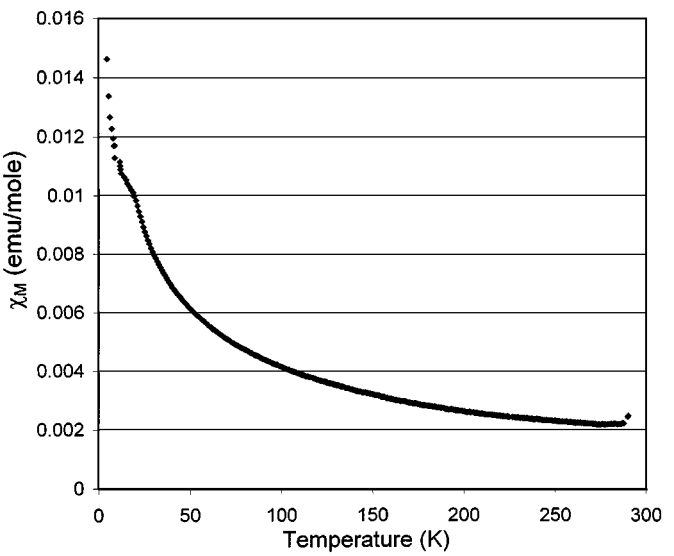

FIG. 4. Molar magnetic susceptibility χ_M (emu/mol) of $TlSr_2NiO_{4+\delta}$ over the temperature range 300–4 K.

$TlSr_2NiO_{4+\delta}$ exhibits paramagnetic behavior and the data can be fitted to the Curie–Weiss equation in the temperature range 300–80 K. This yields a $\mu_{eff} = 2.48\mu_B$ indicative of $\sim$1.5 free electrons per nickel atom, a reasonable value for nickel in oxidation states of Ni^{2+} and Ni^{3+} in a mixture of coordination geometries. The material deviates from Curie–Weiss behavior below 80 K with a weak antiferromagnetic transition occurring at around 15.

CONCLUSIONS

$TlSr_2NiO_{4+\delta}$ has been synthesized and its structure determined using low-temperature neutron powder diffraction. Results reveal that the subcell structural model previously reported (18) could be improved. The observation of ordered oxygen vacancies led to the introduction of a doubled-*b* superstructure model previously reported for the isomorphic $TlSr_2CuO_y$ (16). Refinement of the fractional occupancies of the basal oxygen sites revealed an alternating array of NiO_6 octahedra and NiO_4 square planes along the *b* direction. $TlSr_2NiO_{4+\delta}$ exhibits disorder in the thallium–oxygen layer similar to that observed in high-T_c single-layer thallium copper oxide phases. The final refined stoichiometry of $Tl_{1.78}Sr_4Ni_2O_{9.36}$ yields a nickel oxidation state $\sim$2.7+ .Magnetic susceptibility data reveal the material to be paramagnetic with a small anomaly at $\sim$15 K. A comparison of the metal environment between $TlSr_2NiO_{4+\delta}$ and $TlSr_2CuO_y$ shows a greater distortion in the copper–oxygen coordination due to the Jahn–Teller effect.

$TlSr_2NiO_{4+\delta}$ provides further illustration of the ability of nickel to adopt structural analogues of well-known copper oxide materials. The material demonstrates a remarkable degree of structural correlation with the cuprate analogue, displaying unidirectional ordering of oxygen vacancies in the basal Ni–O layer. The similarities between copper and nickel phases often extend to the magnetic and electrical properties of the materials. It is hoped that the exploration of transition metal materials such as $TlSr_2NiO_{4+\delta}$, which are related to high-T_c copper oxide phases, may help in the understanding of the phenomena of superconductivity and lead to new layered transition metal oxides with unusual electronic or magnetic properties.

ACKNOWLEDGMENTS

The authors acknowledge of EPSRC for providing a studentship for C.S.K and a grant-in-aid for this work; the Institut Laue Langevin for neutron beam time and technical help; and Dr. D. T. Adroga, Physics Department, University of Southampton, for the collection of VSM data.

REFERENCES

1. M. James and J. P. Attfield, *J. Mater. Chem.* **6,** 57 (1996).
2. J. Gopalakrishnan, G. Colsmann, and B. Reuter, *J. Solid State Chem.* **22,** 145 (1977).
3. H. Rieck and R. Hoppe, *Z. Anorg. Allg. Chem.* **392,** 193 (1972).
4. W. Losert and R. Hoppe, *Z. Anorg. Allg. Chem.* **379,** 234 (1970).
5. M. A. G. Aranda and J. P. Attfield, *Angew. Chem. Int. Ed. Engl.* **32,** 1454 (1993).
6. R. Gottscall and R. Scollhorn, *Solid State Ionics* **59,** 93 (1993).
7. M. James and J. P. Attfield, *Chem. Eur. J.* **2,** 737 (1996).
8. D. B. Currie, M. T. Weller, and R. D. Oldroyd, *Physica C* **235,** 441 (1994).
9. A. M. Balagurov, J. Piechota, and A. Pajaczkowska, *Solid State Commun.* **78,** 407 (1991).
10. K. Ishida, Y. Kitaoka, N. Ogata, T. Kamino, K. Asayama, J. R. Cooper, and N. Athanassopoulou, *Physica B* **188,** 1015 (1993).
11. D. M. Ogborne and M. T. Weller, *Physica C* **220,** 389 (1994).
12. D. M. Ogborne and M. T. Weller, *Physica C* **230,** 153 (1994).
13. J. S. Kim, J. S. Swinnea, and H. F. Steinfink, *J. Less-Common Met.* **156,** 347 (1989).
14. D. Kovatcheva, A. W. Hewat, N. Rangavittal, V. Manivannan, T. N. Guru Row, and C. N. R. Rao, *Physica C* **173,** 444 (1991).
15. A. K. Ganguli and M. A. Subramanian, *J. Solid State Chem.* **93,** 250 (1991).
16. E. Ohshima, M. Kikuchi, F. Izumi, K. Hiraga, T. Oku, S. Nakajima, N. Ohnishi, Y. Morii, S. Funahashi, and Y. Syono, *Physica C* **221,** 261 (1994).
17. M. Coutanceau, J. P. Doumerc, J. C. Grenier, P. Maestro, M. Pouchard, and T. Seguelong, *C. R. Acad. Sci. Paris Ser. IIb* **320,** 675 (1995).
18. C. S. Knee and M. T. Weller, *J. Mater. Chem.* **6,** 1449 (1996).
19. A. C. Larson and R. B. Von Dreele, MS-H805, Los Alamos National Laboratory, Los Alamos, NM.
20. L. Koester, H. Rauch, and E. Seymann, *At. Data Nucl. Data Tables* **49,** 65 (1991).
21. Y. Takeda, R. Kanni, M. Sakano, and O. Yamamoto, *Mater. Res. Bull.* **25,** 293 (1989).
22. B. Morosin, E. L. Venturini, and D. S. Ginley, *Physica C* **183,** 90 (1991).